Journal of Nanobiotechnology

RESEARCH

Open Access

Localized DNA tetrahedrons assisted catalytic hairpin assembly for the rapid and sensitive profiling of small extracellular vesicle-associated microRNAs

Ye Zhang[1,2*†], Wenbin Li[1,2†], Tingting Ji[1,2†], Shihua Luo[5†], Jiuxiang Qiu[1,4], Bo Situ[1,2], Bo Li[1,2], Xiaohe Zhang[1,2], Tiange Zhang[1,2], Wen Wang[1,2], Yunju Xiao[6], Lei Zheng[1,2,3*] and Xiaohui Yan[1,2*]

Abstract

The profiling of small extracellular vesicle-associated microRNAs (sEV-miRNAs) plays a vital role in cancer diagnosis and monitoring. However, detecting sEV-miRNAs with low expression in clinical samples remains challenging. Herein, we propose a novel electrochemical biosensor using localized DNA tetrahedron-assisted catalytic hairpin assembly (LDT-CHA) for sEV-miRNA determination. The LDT-CHA contained localized DNA tetrahedrons with CHA substrates, leveraging an efficient localized reaction to enable sensitive and rapid sEV-miRNA measurement. Based on the LDT-CHA, the proposed platform can quantitatively detect sEV-miRNA down to 25 aM in 30 min with outstanding specificity. For accurate diagnosis of gastric cancer patients, a combination of LDT-CHA and a panel of four sEV-miRNAs (sEV-miR-1246, sEV-miR-21, sEV-miR-183-5P, and sEV-miR-142-5P) was employed in a gastric cancer cohort. Compared with diagnosis with single sEV-miRNA, the proposed platform demonstrated a higher accuracy of 88.3% for early gastric tumor diagnoses with higher efficiency (AUC: 0.883) and great potential for treatment monitoring. Thus, this study provides a promising method for the bioanalysis and determination of the clinical applications of LDT-CHA.

Keywords: DNA tetrahedron, Catalyzed hairpin assembly, sEV-miRNAs, Early cancer diagnostics

†Ye Zhang, Wenbin Li, Tingting Ji and Shihua Luo contributed equally to this work

*Correspondence: Zhangye232@i.smu.edu.cn; nfyyzhenglei@smu.edu.cn; gzyanxh@126.com

[1] Laboratory Medicine Center, Department of Laboratory Medicine, Nanfang Hospital, Southern Medical University, Guangzhou 510515, Guangdong, China
Full list of author information is available at the end of the article

Graphical Abstract

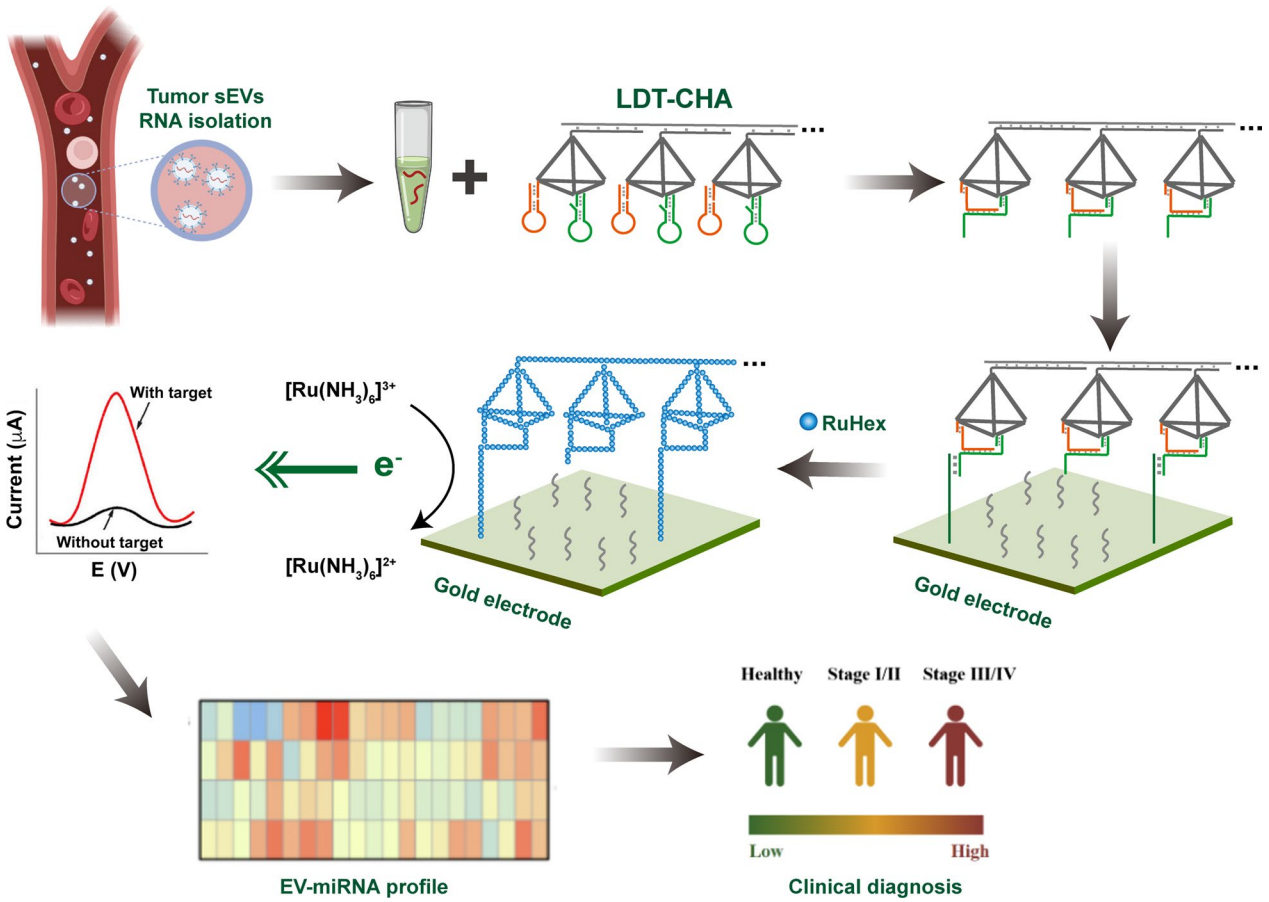

Introduction

Small extracellular vesicles (sEVs) with sizes ranging from 30 to 200 nm are lipid bilayer-packaged membrane vesicles shed by almost all cell types [1]. They can transmit valuable biological information to recipient cells by transferring intravesicular biomolecules from their parental cells [2]. MicroRNAs (miRNAs) are a class of noncoding RNAs that can be largely enclosed in sEVs [3]. They bind to target mRNAs to regulate gene expression, which participates in the occurrence and development of many diseases [4–6]. Compared to free miRNAs, EV-miRNAs can be more stably detected in circulation owing to their protection by sEV lipid membranes, which makes them potential biomarkers for cancer diagnosis [7, 8].

At present, the conventional method for sensitive sEV-miRNA determination is reverse transcription quantitative polymerase chain reaction (RT–qPCR) [9]. However, the clinical application of RT–qPCR is greatly impeded due to the tediousness of operation, specialized experimental equipment required, and high false positive rate [10, 11]. In this regard, multiple methods have been proposed for sEV-miRNA analysis, such as the use of nanomaterial-based technologies [12–14], enzyme-assisted strategies [15–17], and spherical nucleic acid [18–20]. Despite their decent performances, these strategies are not rapid and simple enough for sEV-miRNAs measurement because of the tedious operation and harsh reaction conditions. Accordingly, metastable hairpin-driven amplification, including catalytic hairpin assembly (CHA) [21–23], hybridization chain reaction (HCR) [24, 25], have been proposed due to its high specificity, low-cost, and easy to use. Compared with the assembled concatemer products of HCR, the dangled ssDNA products of CHA are easier to capture and generate an enhanced electrochemical signal [18, 26, 27]. However, the deficient sensitivity and inefficiency hindered the practical application of metastable hairpin-driven amplification.

In order to improve the sensitivity of metastable hairpin-driven amplification, multiple amplification were proposed [28–30]. Such as, Peng et al. proposed a multiple amplification strategy by integrating CRISPR-Cas12a and CHA for miRNAs detection [31]. Zhang et al. designed a cascade amplification method based on CHA and HCR for miRNA detection [32]. Zhang et al. proposed a multi-layers DNA tetrahedron-assisted CHA for miRNA detection [33]. Although the sensitivity of these strategies were improved, their may suffer from some disadvantages: (i) multiple steps results in prolonged and tedious procedure; (ii) time-consuming process of multiple metastable hairpin-driven amplification and rigorous reaction conditions of enzyme-assist metastable hairpin-driven amplification restrict their practical applications; and (iii) the incompatible reaction conditions led to serious signal leakage.

Herein, we designed a novel electrochemical platform based on localized DNA tetrahedron-assisted catalytic hairpin assembly (LDT-CHA) for sensitive sEV-miRNA detection. Compared with other metastable hairpin-driven amplification strategies, our methods have multiple advantages. Firstly, DNA tetrahedron-assisted catalytic hairpin assembly (DT-CHA) could increase the local concentrations of CHA substrates by confining hairpins in a compact space, which dramatically improve the amplification efficiency. Secondly, the LDT-CHA contained a number of DT-CHAs as successive reactants in a confined space, which could minimize leakage of CHA by the precise-control space of each DT-CHA. Thirdly, The LDT could act as programmed track, once the driving motor is triggered by a target sEV-miRNA, the sEV-miRNA would move along the LDT-CHA to produce cascaded signal output. As a proof-of-concept, sEV-miR-1246 was employed as a model molecule because of its high expression in gastric tumour sEVs[34, 35]. The LDT-CHA was associated with DNA nanowires, DNA tetrahedrons, and the CHA system (H1 and H2). The DNA tetrahedrons contained four DNA strands (S1–S4). The 3′ sticky ends of S3 and S4 were adopted to anchor with CHA reactants (Scheme 1A). First, the sticky end C in H2, which could bind to the capture probe, was blocked. The LDT-CHA was established by hybridization of DNA tetrahedron-CHA (DT-CHA) to a DNA nanowire with repeated sequence. The sEV-miRNAs hybridized with one H1 in DT-CHA to trigger the CHA along the DNA nanowire due to the arrangement of DNA tetrahedrons in LDT-CHA and the programmed space. Next, multiple sticky end Cs were exposed by H1-H2 assembly on the tetrahedron and hybridized with the capture probe. Then, an amplified signal for the determination of sEV-miRNAs was generated by the electroactive substance RuHex, which links with the captured tandem tetrahedrons by electrostatic interactions (Scheme 1B). The proposed platform based on LDT-CHA holds great potential for sEV-miRNA detection and clinical application for cancer diagnostics.

Characterization of the LDT-CHA

The successful assembly of LDT-CHA was first confirmed by agarose gel electrophoresis. As shown in Fig. 1A, the probes were combined into DNA tetrahedron (Lane 1 to 3), DT-CHA (Lane 4), and LDT-CHA (Lane 6). Notably, in the presence of target miRNA, a more complex spatial structure of DT-CHA was generated, and the electrophoretic mobility was reduced (Lane 5). Atomic force microscopy (AFM) was used to reveal the morphologies of the LDT-CHA, showing a larger ordered arrangement of linked patterns (Fig. 1B, Additional file 1: Fig. S1) than that of the DT-CHA (Additional file 1: Fig. S2). The molecular size increased from 3 nm for DT-CHA to 105 nm for LDT-CHA, as suggested by DLS (Fig. 1C). Compared with DT-CHA, the zeta potential distribution of LDT-CHA decreased from − 2.3 to − 6.5 mV because of the enhanced negative electricity of the localized DT-CHA assembly (Fig. 1D). These results demonstrated that LDT-CHA was successfully prepared with high yield.

The feasibility of LDT-CHA

The superior features of LDT-CHA were first confirmed by DPV measurement. Compared with DT-CHA, the DPV signal of LDT-CHA was improved almost three-fold, and the background signal was almost unchanged (Fig. 2A). This means that LDT-CHA obtained higher sensitivity and a wider linear range than DT-CHA for sEV-miRNA analysis. We used fluorescence signal measurements to further confirm the amplification of LDT-CHA. The hairpin DNA H1 modified with energy donor FAM and receptor BHQ1 at both ends is designed to release fluorescence in response to the target. As shown in Fig. 2B, the time-dependent fluorescence signal substantially increased with the addition of miRNA-1246. The fluorescence plateau of LDT-CHA was obtained in 10 min, and the signal of LDT-CHA was almost 2 times higher than that of DT-CHA, which is consistent with the electrochemical outcomes. These results demonstrated the high sensitivity and minimized leakage of LDT-CHA.

The outstanding sensitivity of LDT-CHA was confirmed based on collision theory ($V = 1/cN$), in which N represents the Avogadro constant, C represents the concentration of reactants, and V represents the local sphere volume. When the solution of the traditional CHA system included 25 nM H1 and 25 nM H2, the volume of collision space was calculated to be 6.6×10^{-17} L (Fig. 2C). After CHA was tied to the DNA tetrahedron

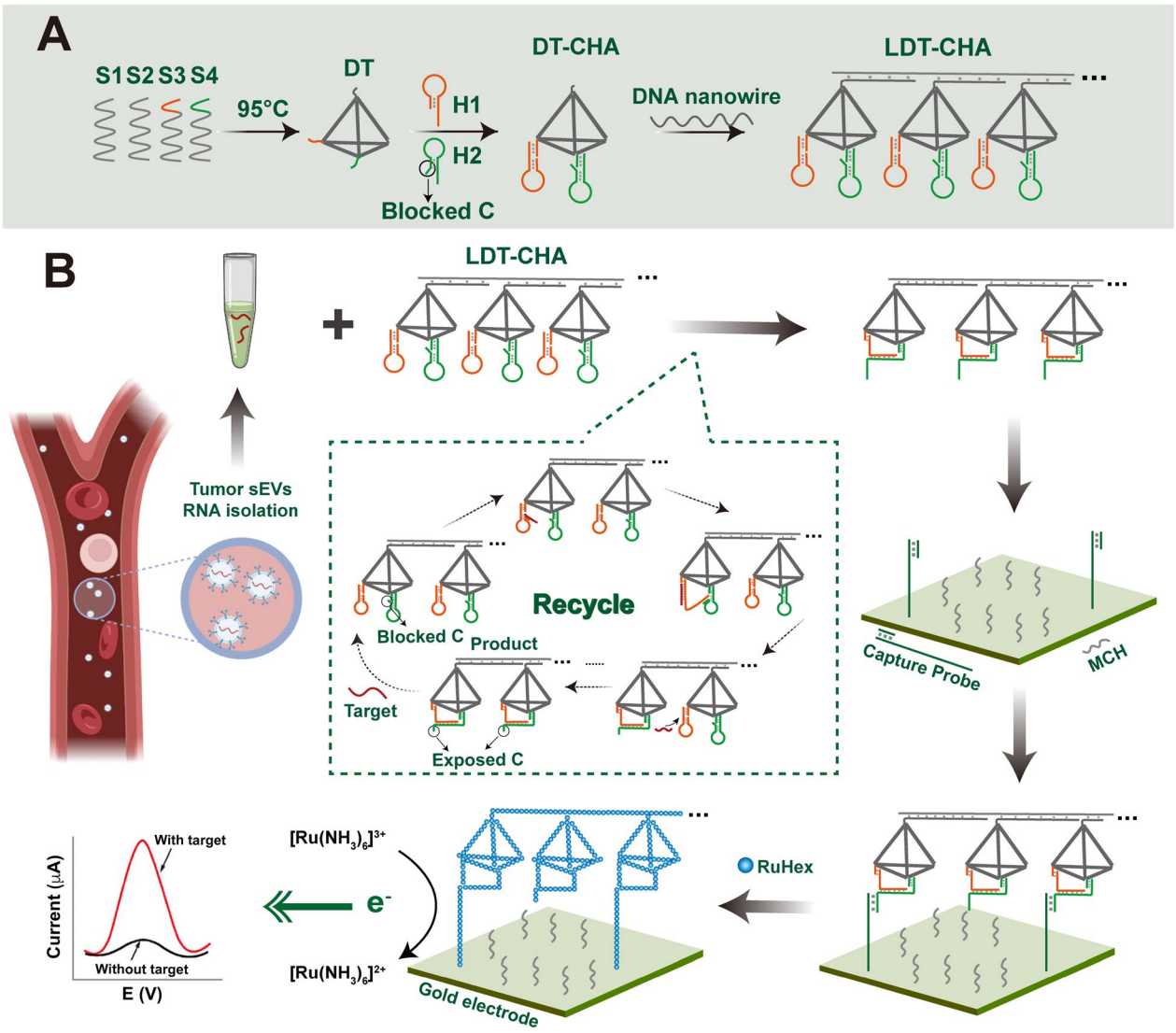

Scheme 1 Schematic principle of the electrochemical biosensor for sEV-miRNAs determination. **A** Assembly process of LDT-CHA. **B** The reaction of LDT-CHA on the surface of electrode

(DT-CHA), the distance between H1 and H2 was shortened to 5.78 nm (17 bp). Then, the local concentrations of H1 and H2 were both elevated to 2.0 mM. Similarly, supposing that the solution contains 25 nM DT-CHA, the distance between DT-CHA was reduced to 3.74 nm. According to the analytical formula $V = 1/cN$, the space for the two DT reaction units was 1.65×10^{-17} L, and the local concentration was elevated to 1.0 mM. The direct correlation of collision frequency to hairpin concentration indicates that the enhanced reaction kinetics of LDT-CHA were caused by the increased local concentration.

The balance between the localized reaction and leakage reaction plays a vital role in LDC because of the DNA breath reaction. In the LDT-CHA system, the CHA breath reaction depends on the distance between hairpins (H1 and H2), which are connected by a DNA tetrahedron (Fig. 2D). To study the effect of the distance between H1 and H2 on the DNA tetrahedron, three DNA tetrahedrons with distances of 13, 17 and 26 base pairs (13-DT, 17-DT, and 26-DT) were synthesized. As shown in Fig. 2E, the 17 bp TDs had the best performance in the signal-to-noise ratio. In contrast, the 13 bp TD had a high background signal, and the 26 bp TD had low efficiency for the CHA reaction. Thus, the 17 bp TD was chosen as the best design. To study the effect of distance between DNA tetrahedrons,

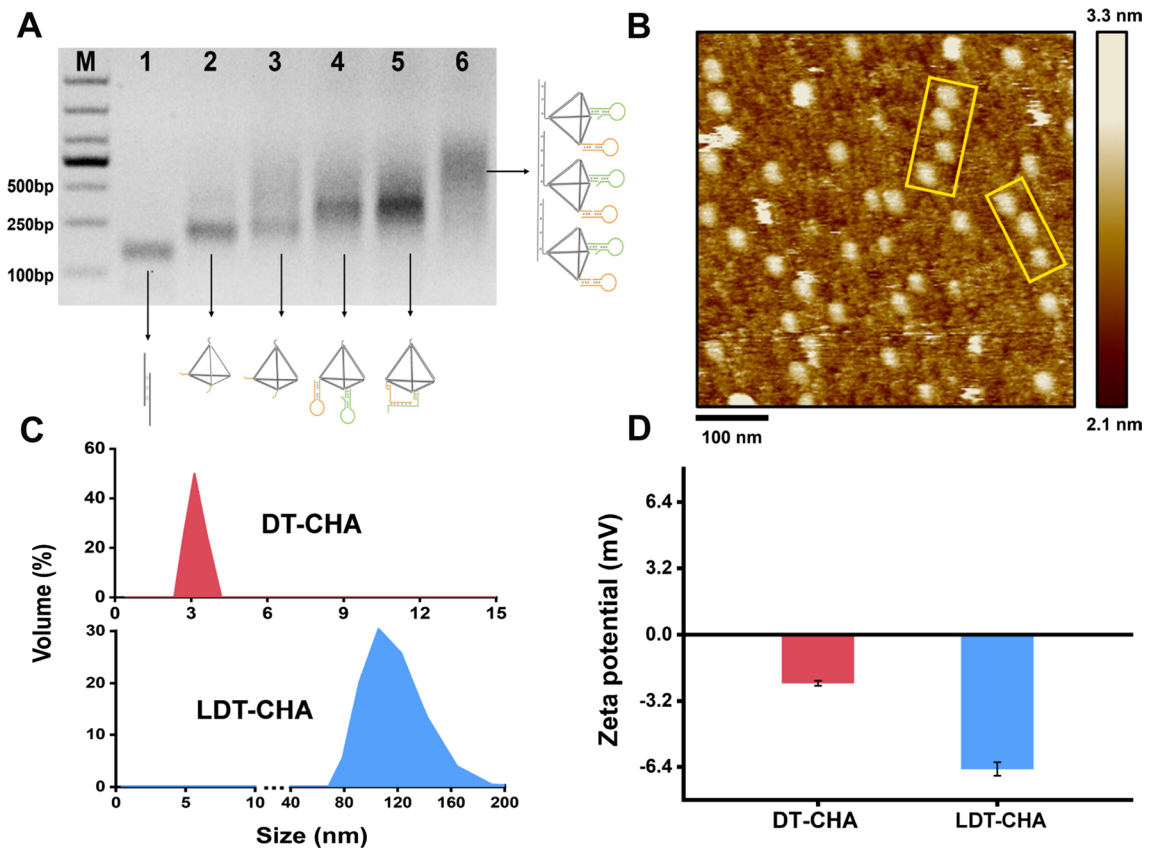

Fig. 1 Characterization of the LDT-CHA. **A** Gel electrophoresis analysis of LDT-CHA assembly process. Lane M: 1000 bp marker; Lane 1: S1/S2; Lane 2: S1/S2/S3; Lane 3: S1/S2/S3/S4; Lane 4: S1/S2/S3/S4/H1/H2; Lane 5: S/S2/S3/S4/H1/H2/miR-1246; Lane 6: S1/S2/S3/S4/H1/H2/nanowire. **B** Atomic force microscope imaging of LDT-CHA. **C** Dynamic light scattering of DT-CHA and LDT-CHA particle size. **D** Zeta potential analysis of DT-CHA and LDT-CHA nanoparticles

three different distances were designed (Fig. 2F). The 10 bp distance had a high efficiency in the signal-to-noise ratio because the steric hindrance of the CHA system was reduced by the three-dimensional structure of the DNA tetrahedron.

Characterization of the electrochemical biosensor

To confirm the assembly of LDT-CHA on the electrode surface, we characterized the electrochemical biosensor by EIS and SWV analysis. In the EIS measurements, the diameter of the semicircle on the curve reflects the electron transfer resistance proportionally (Ret). As demonstrated in Fig. 3A, the bare gold surface line was almost straight (curve a), indicating the good electrical conductivity of the gold electrode with low Ret. We next modified the gold electrode with double-strand capture probes via Au–S intermolecular interactions, resulting in larger DNA backbone aggregation. The $[Fe(CN)_6]^{3-/4-}$molecules were alienated to the electrode surface, resulting in an increase in Ret (curve b). Then, MCH was used to block the redundant sites of the electrode, which greatly increased Ret due to the steric effect of the large molecule (curve c). With the addition of target miRNA, the LDT-CHA combined the capture probe on the surface of the electrode showed greater Ret (curve e) than that of DT-CHA (curve d). SWV (Fig. 3B) analyses also demonstrated the step-by-step assembly of the electrode, which is consistent with the EIS results. These results indicate the successful assembly of the proposed biosensor and the powerful amplification of LDT-CHA.

Analytical performance of the biosensor

Before demonstrating the properties of the proposed biosensor, some key conditions were optimized, as shown in Additional file 1: Figs. S3 and S4. Then, we studied the analytical performance, including sensitivity, specificity, and reproducibility, using DPV measurements. To exhibit the superior sensitivity of LDT-CHA, the DPV signals of LDT-CHA (Fig. 4A), DT-CHA (Fig. 4D), and CHA (Additional file 1: Fig. S5) in response to sEV-miR-1246

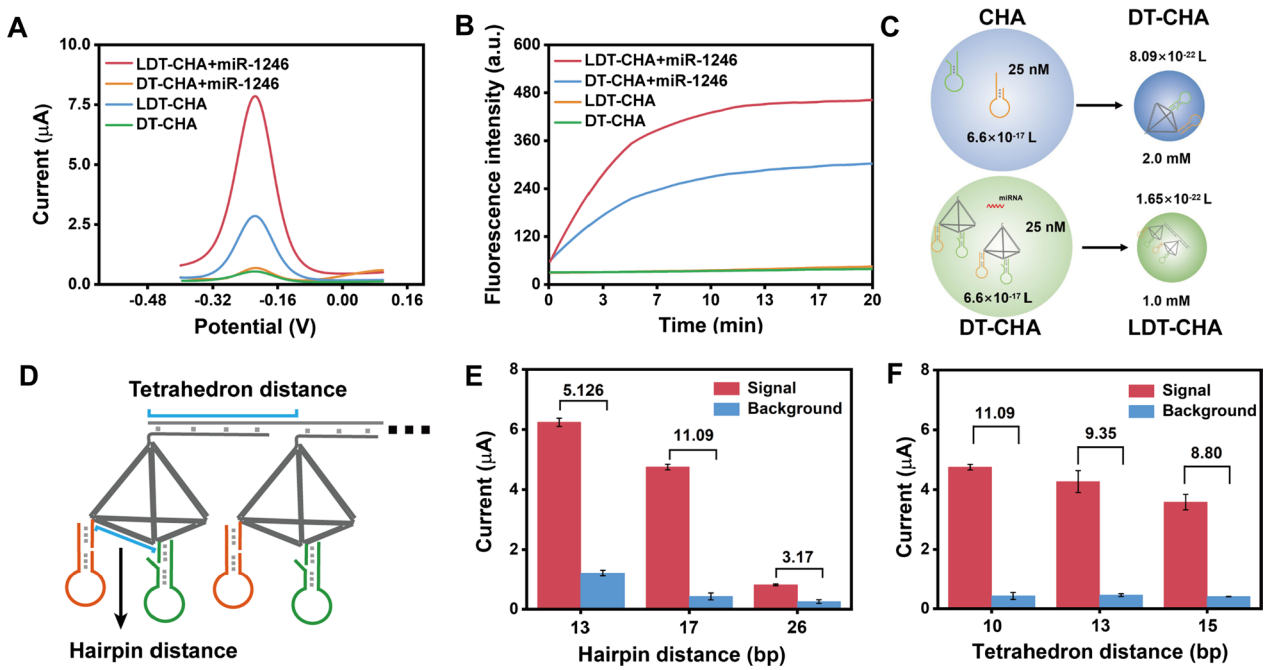

Fig. 2 **A** DPV analysis and **B** Fluorescence kinetics monitoring of LDT-CHA and DT-CHA. **C** Comparison of the reaction space and local concentration of traditional CHA and DT-CHA (upper), DT-CHA and LDT-CHA (lower). **D** The scheme of LDT-CHA with different distance of hairpins and Tetrahedrons. **E** Signal-to-noise ratio of the LDT-CHA with different hairpins distance in the presence of 10 nM miR-1246. **F** Signal-to-noise ratio of the LDT-CHA with different tetrahedrons distance in the presence of 10 nM miR-1246

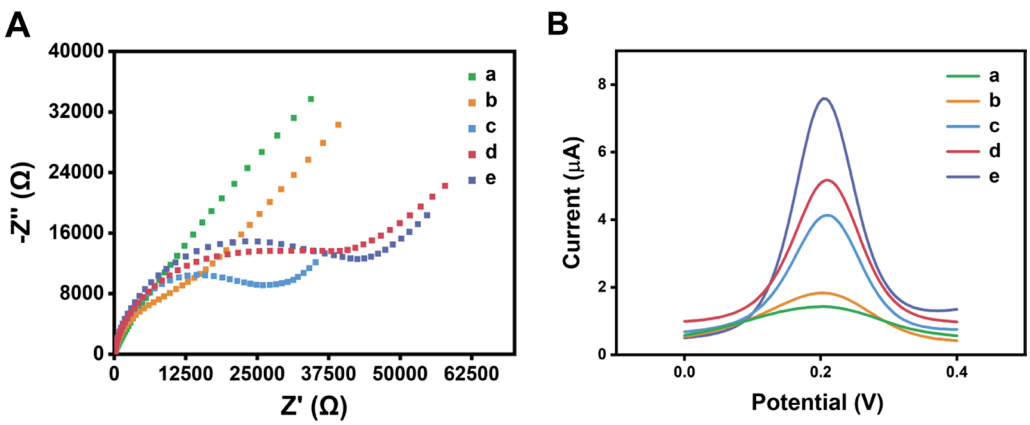

Fig. 3 **A** EIS and **B** SWV of the bare gold electrode (**a**); the electrode modified with capture probe (**b**); the modified electrode after MCH block (**c**); DT-CHA captured by the prepared electrode (**d**); LDT-CHA captured by the prepared electrode (**e**)

were detected. With increasing sEV-miR-1246 concentrations, the DPV signals of LDT-CHA (Fig. 4B) were greatly enhanced compared to those of DT-CHA (Fig. 4E) and CHA (Additional file 1: Fig. S5B). Moreover, the LDT-CHA had a broad linear range from 100 aM to 10 pM with a correlation equation fitted as $I = 0.438\ lgC_{target} + 2.163$ ($R^2 = 0.993$) (Fig. 4C). Based on the 3SD principle, the limit of detection of LDT-CHA was obtained at 21 aM, which was 7790-fold lower than that of DT-CHA (Fig. 4F) and 173616-fold lower than that of CHA (Additional file 1: Fig. S5C), demonstrating the enhanced sensitivity of the LDT-CHA strategy.

The specificity of the platform was measured using different groups of sEV-miRNAs containing a single-base mismatch sequence (SM), double-base mismatch sequence (DM), random sequence (RS), and

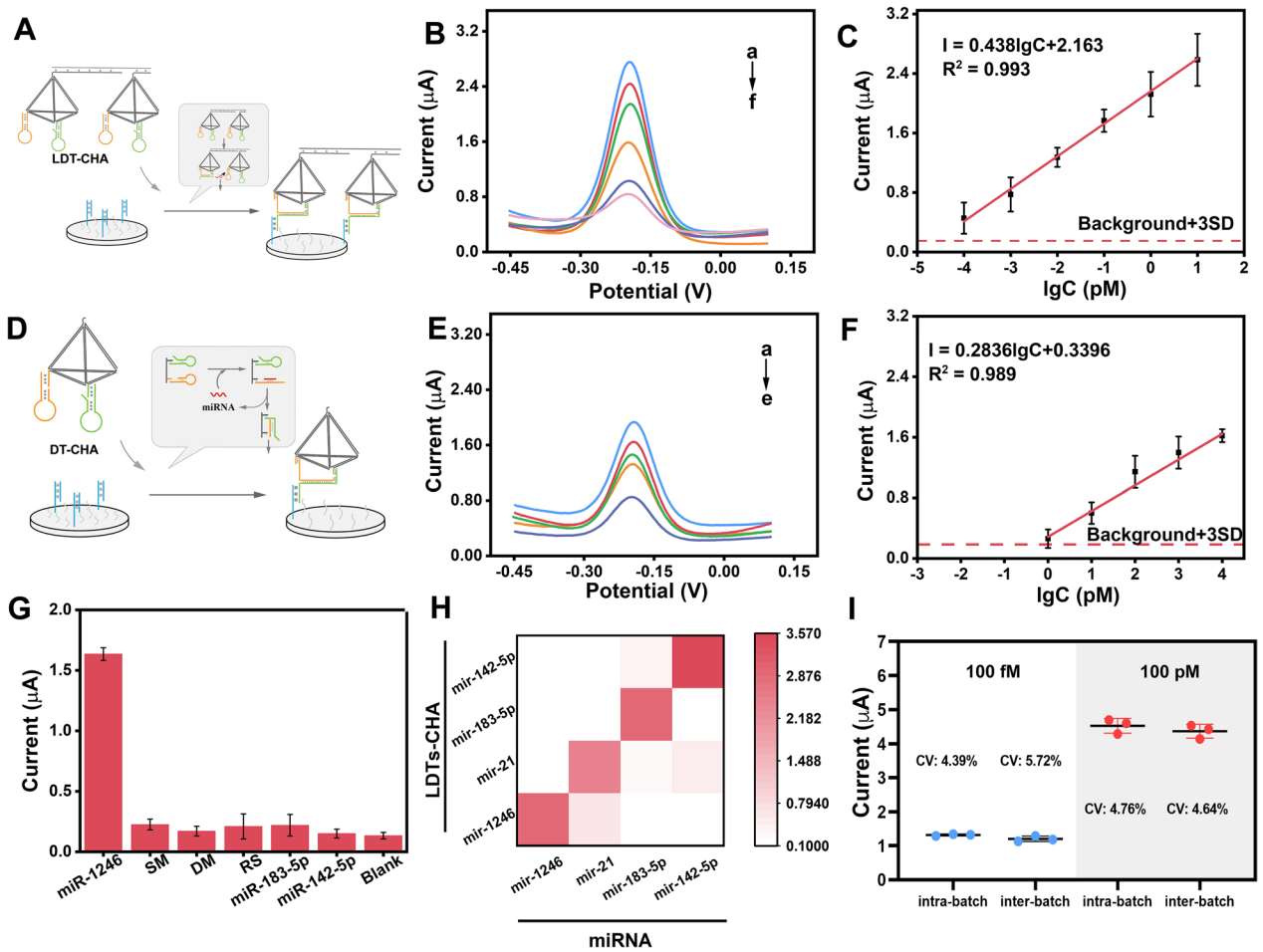

Fig. 4 **A** Schematic illustration of the LDT-CHA strategy. **B** DPV responses and **C** corresponding calibration curve of target miRNA with the concentration from 100 aM to 10 pM (a: 10 pM; b: 1 pM; c: 0.1 pM; d: 0.01 pM; e: 0.001 pM; f: 0.0001 pM) using LDT-CHA. **D** Schematic illustration of the DT-CHA strategy. **E** DPV responses (**F**) and corresponding calibration curve (**F**) of target miRNA with the concentration from 1 fM to 10 nM (a: 10 nM; b: 1 nM; c: 100 pM; d: 10 pM; e: 1 pM) using DT-CHA. **G** DPV results respond to target miRNA and five interferences. **H** Heat map analysis of the orthogonal identification of four sEV-miRNAs. **I** Stability of the LDT-CHA. The error bars are the standard deviations by three repetitive assays (n = 3)

several homologous sEV-miRNAs (sEV-miR-21, sEV-miR-183-5P, and sEV-miR-142-5P). As exhibited in Fig. 4G, the electrochemical signal of miR-1246 was almost 10 times higher than those of mismatched sequences and other sEV-miRNAs, indicating the high specificity of the electrochemical platform. The specificity of LDT-CHA was confirmed further using orthogonal identification of four sEV-miRNAs of LDT-CHA. As shown in Fig. 4H, only the appropriate LDT-CHA response to correct sEV-miRNAs generated an enhanced signal. To explore the reproducibility of the proposed biosensor, the samples containing 100 fM and 100 pM target miRNA were tested in regards to interbatch and intrabatch variability, respectively. The variable coefficient of the result was approximately 6% (Fig. 4I), indicating a suitable reproducibility of this platform. Next, to evaluate the stability of the proposed platform, the biosensor was measured in the presence of 10 nM miRNA-1246 for 8 days. The electrochemical signals of the initial measurement were maintained at 85.4% (Additional file 1: Fig. S6).

Determination of sEV-miRNAs in cell lines

Before the determination of the sEV-miRNAs, the standard ultracentrifugation method was adopted for separating EVs derived from a gastric tumour cell line (MKN-28). The represented EV derived from the MKN-28 cell line was characterized by a standard protocol. Typical partially collapsed discs with diameters of 110 nm are shown in TEM images (Fig. 5A). The NTA exhibited a group ranging from 51 to 208 nm with a peak at 110 nm (Fig. 5B). The specific protein markers

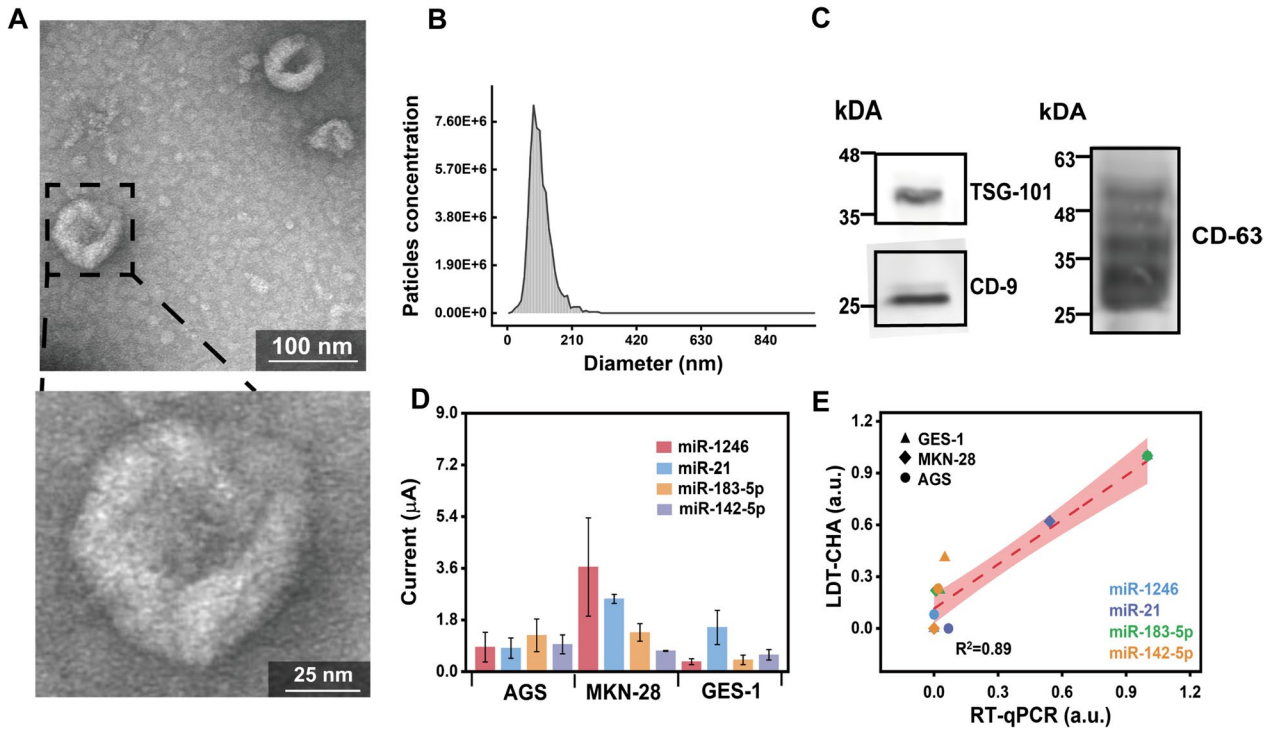

Fig. 5 **A** TEM images of model sEV isolated from MKN-28 cell lines (scale bar: 100 nm (upper) and 50 nm (lower)). **B** Size distribution analysis of MKN-28 cell sEV. **C** The expression of specific sEV proteins by Western blot analysis. **D** DPV measurements for four sEV-miRNAs expression in sEV derived from MKN-28, AGS, and GES-1 cell lines. **E** The correlation between LDT-CHA and RT-qPCR method for detecting four sEV-miRNAs expression in sEV derived from MKN-28, AGS, and GES-1 cell lines. The bright red-dashed line indicates the best linear fit in the log–log scale, and the shaded red area represents the 95% confidence

of EVs (positive proteins: CD9, CD63, and TSG101) were confirmed by Western blotting analysis (Fig. 5C). These results indicated the high purity and integrity of the isolated EV.

Then, the sEVs derived from two gastric tumour cell lines (MKN-28 and AGS) and a normal gastric epithelial cell line (GES-1) were separated to extract total RNA. The proposed platform was adopted to measure the panel of four gastric tumour-associated sEV-miRNAs (sEV-miR-1246, sEV-miR-21, sEV-miR-183-5p, and sEV-miR-142-5p). As shown in Fig. 5D, the expression levels of the four sEV-miRNAs in various EVs were different, and most of them were much higher in sEVs from gastric tumour cell lines than in those from the normal epithelial cell line, especially those of sEV-miR-1246 and sEV-miR-183-5p. qRT–PCR was adopted to further determine the expression levels of the sEV-miRNAs and compare the obtained results with those obtained by the electrochemical platform, which were consistent with those of our developed biosensor ($R^2 = 0.89$) (Fig. 5E). These results indicate the application potential and accuracy of the developed electrochemical biosensor.

Clinical sample analysis

To explore the clinical applications of the proposed biosensor, a gastric cancer patient cohort (n = 57; 35 patients with stage I-II disease, 10 patients with stage III-IV disease, and 12 healthy donors as controls) was developed (Additional file 1: Table S2). sEV-miRNA was isolating after EVs separation by ultracentrifugation. The sEV-miRNA expression profiles are summarized in Fig. 6A. As shown in Fig. 6B–E, the average levels of all four sEV-miRNAs were highest in patients with stage III-IV disease, and sEV-miR-142-5p had the best capacity for distinguishing gastric cancer from healthy donor samples ($p < 0.05$). However, the two distributions of the patients with stage I-II disease and healthy donors overlapped, which made identification based on a single sEV-miRNA difficult. To improve the clinical performance of the biosensor for cancer diagnosis, we proposed using a combination of sEV-miRNAs and analysing the ROC curves. Compared to the single sEV-miRNA (Fig. 6F and H), the combination of four sEV-miRNAs showed higher accuracy (AUC: 0.904, 95% CI 0.808 to 0.999) for discriminating patients with gastric cancer from healthy donors (Fig. 6G and Additional

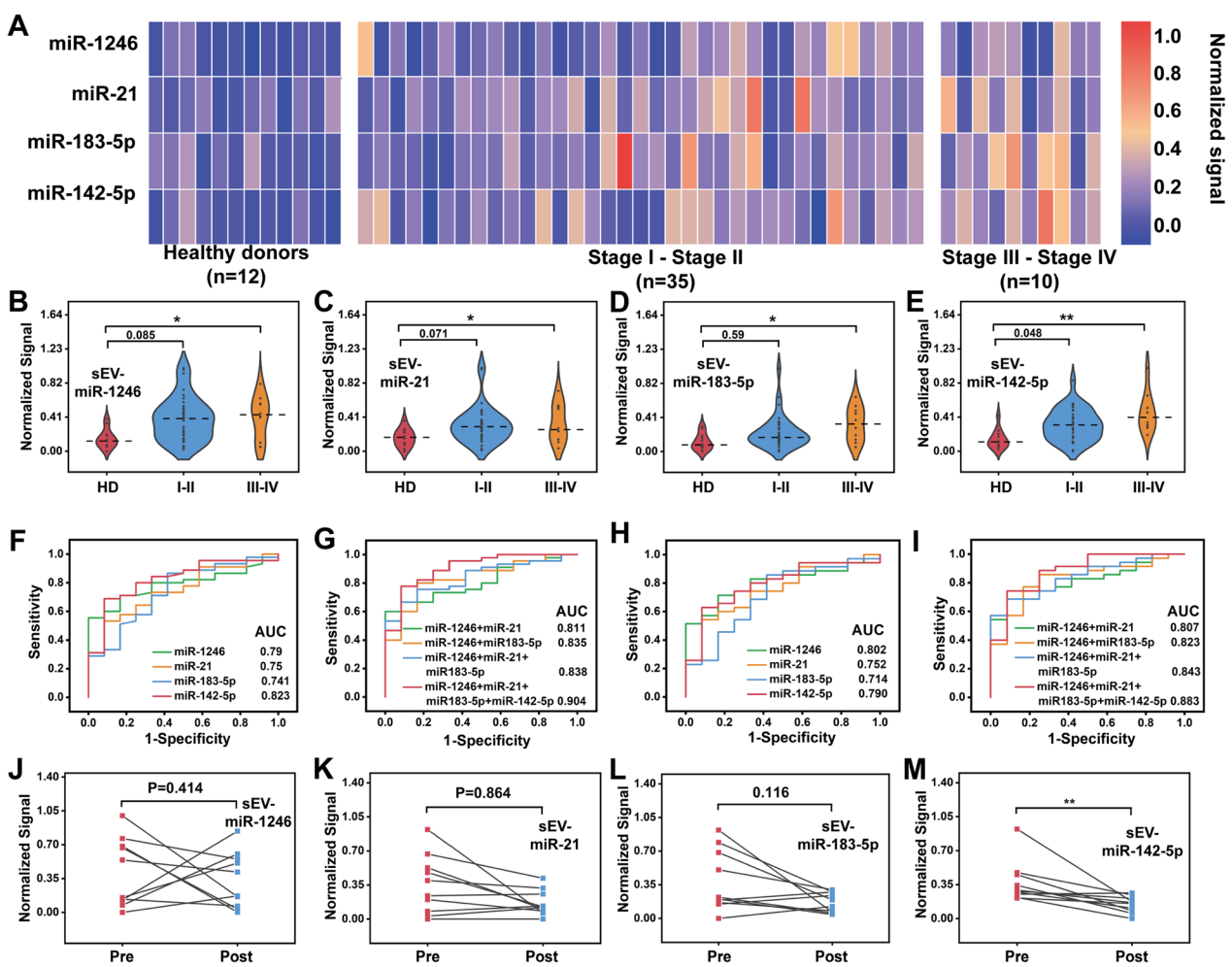

Fig. 6 **A** The expression of four sEV-miRNAs measured by the electrochemical platform in gastric cancer cohort (healthy donors, n = 12; patients with gastric cancer in stage I–II, n = 35; stage III–IV, n = 10. **B**–**E** The electrochemical signal for sEV-miR-1246, sEV-miR-21, sEV-miR-183-5p and sEV-miR-142-5p profiling in gastric cancer cohort (*p < 0.1; **p < 0.05). **F**, **G** ROC curve of single sEV-miRNA and combined sEV-miRNAs for diagnosing patients with gastric tumors. **H**, **I** ROC curve of single sEV-miRNA and combined sEV-miRNAs for identifying gastric cancer in early stages (I–II). **J**–**M** Plasma samples from gastric cancer patients (n = 9) before (Pre) and after (Post) surgery measured by sEV-miRNAs profiles (**J** sEV-miR-1246; **K** sEV-miR-21; **L** sEV-miR-183-5p; and **M** sEV-miR-142-5p; **p < 0.05)

file 1: Fig. S7). Moreover, the combination of four sEV-miRNAs showed a sensitivity of 74.3% and a specificity of 66.0% (AUC: 0.883, 95% CI 0.772 to 0.995) for the identification of gastric cancer with stages I-II (Fig. 6I and Additional file 1: Fig. S8).

To further demonstrate the clinical applicability of this biosensor, the sEV-miRNA profile changes were tracked in patients who underwent clinical treatment (Additional file 1: Table S3). We compared sEV-miRNA expression before and after the operation. The expression levels of sEV-miR-1246 (Fig. 6a), sEV-miR-21 (Fig. 6b), and sEV-miR-183-5p (Fig. 6d) showed no significant changes, with P values of 0.414, 0.864, and 0.116, respectively (paired t test). In contrast, sEV-miR-142-5p decreased in all patients (Fig. 6c) (P < 0.01, paired t test); thus, it may be used as a candidate marker for treatment monitoring.

Discussion

The sEV-miRNA in the circulation is promising biomarkers for cancer diagnostics. However, most methods for sEV-miRNA measurement require sophisticated operation and expensive equipment. Here, we present a rapid and sensitive electrochemical biosensor based localized DNA carrier and catalytic hairpin assembly for rapid determination of multiple sEV-miRNAs with high sensitivity and selectivity in clinical samples. For the nucleic acid amplification of LDT-CHA, The DNA nanowire

confined DT-CHA in a compact space accelerating the CHA amplification by DNA tetrahedron and minimizing leakage of the localized reaction by creating a precise-control space for each DT-CHA, demonstrating superior sensitivity. In this work, LDT-CHA, an metastable hairpin-driven amplifier based on localized DNA tetrahedrons and catalytic hairpin assembly, has been adopted to detect the low expression sEV-RNAs in serum of GC patients. Furthermore, the amplification can be completed in one step, which greatly simplified the operation. By our unique combination of the localized DNA tetrahedrons with the CHA, this platform can measure the target sEV-miRNA down to a concentration of 25 aM within 30 min with high specificity and repeatability. Compared to a previous platform based on metastable hairpin-driven amplification (Additional file 1: Table S4), the proposed electrochemical biosensor based on LDT-CHA has better sensitivity with a short processing time. Although the surface-enhanced Raman-based method has higher sensitivity, its applications are restricted by the tediousness of the process and expensiveness of the equipment.

Moreover, the results we detected by LDT-CHA of sEV-miRNA show difficulty distinguishing GC patients. Thus, multiple sEV-miRNA are necessary for GC diagnosis due to the heterogeneous feature of sEV from patients. Using a four-sEV-miRNA panel, the accuracy of this biosensor was 90% for the discrimination of cancer versus healthy individuals in a clinical cohort (n = 57). The sensitivity, specificity and accuracy to distinguish gastric cancer patients at an early stage are 74, 66 and 88%, respectively. It is worth noting that the sEV-miRNA also demonstrate the potential for effective GC prognostic evaluation, which could further expand clinical applications of this platform. Our next step is to expand the panel of sEV-miRNA and conduct a large-scale validation study to improve the accurate of clinical applications. This platform holds the potential to combined with other strategies, such as separation and microfluidic technology, to realize sEV isolation, signal amplification, and simultaneous detection of multiple sEV-miRNAs on one system, producing a high efficiency 'sample in-result out' biosensor.

Although LDT-CHA need to prepare in advance, it does not need complex operation, sophisticated instrument, or trained personnel, which are required for most of the sEV-miRNA analysis methods at present. Moreover,the total cost of the platform can be as low as $0.32 per test (Additional file 1: Table S5). Overall, the proposed biosensor with features including simple operation, rapid testing, and inexpensive equipment, which will advance point-of-care testing in the field of noninvasive diagnosis and cancer monitoring.

Supplementary Information

The online version contains supplementary material available at https://doi.org/10.1186/s12951-022-01700-6.

Additional file 1. Materials and methods. Figure S1. 3D image of LDT-CHA characterization by atomic force microscopy (AFM). Figure S2. (A) 2D and (B) 3Dimage of DT-CHA characterization by atomic force microscopy (AFM); Scale bars are 1 um. Figure S3. The effect of the reaction time of LDT-CHA. Figure S4. The effectof the incubating temperature of LDT-CHA. Figure S5. (A) Schematic illustration of traditional CHA. (B) DPV respond and corresponding calibration curve from 1 pM to1 nM using traditional CHA. (C) Corresponding calibration curve of target miRNA with the concentration from 10 pM to 100 nM using Traditional CHA, error bars representstandard deviations of the measurements (n = 3). Figure S6. The stability of the proposed LDT-CHA platform, error bars represent standard deviations of the measurements (n = 3).Figure S7. ROC curve of combined sEV-miRNAs for identifying patients with gastric tumors. Figure S8. ROC curve of combined sEVmiRNAsfor identifying patients with early-stage gastric tumors. Table S1. DNA sequences of used in this assay. Table S2. Clinical information for healthy donors (HD) and patients with gastric cancer (GC). Table S3.Clinical information for patients who underwent clinical treatment comparison. Table S4. Comparison of different biosensors for detecting sEV-miRNA. Table S5. Cost analysis.

Acknowledgements
Not applicable.

Author contributions
YZ: conceptualization, writing, experimentation. WL: experimentation, writing. JQ: experimentation. XZ: experimentation. TZ: experimentation. WW: experimentation. YX: experimentation. BL: experimentation. BS: experimentation, writing, editing. LZ: conceptualization, writing, editing. XY: conceptualization, writing, editing. All authors read and approved the final manuscript.

Funding
This study was supported by the the National Key R&D Program of China (2021YFA1300604), the Major State Basic Research Development Program of Natural Science Foundation of Shandong Province in China (ZR2020ZD11), the Key Project of Basic and Applied Basic Research of Guangdong Province (2019B1515120074), the National Natural Science Foundation of China (82072382, 82272424), the National Science Fund for Distinguished Young Scholars of China (82025024), the Major Scientific and Technological Special Project in the Precision Medical Field of Guangdong Province (2019B020232003), the Guang Dong Basic and Applied Basic Research Foundation of China (2021A1515012244).

Availability of data and materials
Not applicable.

Declarations

Ethics approval and consent to participate
All clinical samples used in this study were collected from Nanfang Hospital, Southern Medical University according to the institutional ethical guideline laid down in 1964 Declaration of Helsinki. The study was approved by the regional ethics committee (NFEC-2022-220).

Consent for publication
All authors read and approved the final manuscript.

Competing interests
The authors declare that they have no known competing financial interests or personal relationships that could have appeared to influence the work reported in this paper.

Author details
[1]Laboratory Medicine Center, Department of Laboratory Medicine, Nanfang Hospital, Southern Medical University, Guangzhou 510515, Guangdong,

China. [2]Guangdong Engineering and Technology Research Center for Rapid Diagnostic Biosensors, Nanfang Hospital, Southern Medical University, Guangzhou 510515, China. [3]Department of Clinical Laboratory, Shunde Hospital, Southern Medical University (The First People's Hospital of Shunde), Foshan 528300, Guangdong, China. [4]Department of Laboratory Medicine, Guangzhou Eighth People's Hospital, Guangzhou Medical University, Guangzhou 510515, China. [5]Center for Clinical Laboratory Diagnosis and Research, The Affiliated Hospital of Youjiang Medical University for Nationalities, Baise 533000, Guangxi, People's Republic of China. [6]Division of Laboratory Medicine, Guangdong Provincial People's Hospital, Guangdong Academy of Medical Sciences, Guangzhou 510000, China.

Received: 13 September 2022 Accepted: 8 November 2022
Published online: 01 December 2022

References

1. Tkach M, Thery C. Communication by extracellular vesicles: where we are and where we need to Go. Cell. 2016;164:1226–32.
2. Raposo G, Stahl PD. Extracellular vesicles: a new communication paradigm? Nat Rev Mol Cell Biol. 2019;20:509–10.
3. O'Brien K, Breyne K, Ughetto S, Laurent LC, Breakefield XO. RNA delivery by extracellular vesicles in mammalian cells and its applications. Nat Rev Mol Cell Biol. 2020;21:585–606.
4. Robbins PD, Morelli AE. Regulation of immune responses by extracellular vesicles. Nat Rev Immunol. 2014;14:195–208.
5. Zhang Y, Tan J, Miao Y, Zhang Q. The effect of extracellular vesicles on the regulation of mitochondria under hypoxia. Cell Death Dis. 2021;12:358.
6. Mittal S, Gupta P, Chaluvally-Raghavan P, Pradeep S. Emerging role of extracellular vesicles in immune regulation and cancer progression. Cancers. 2020. https://doi.org/10.3390/cancers12123563.
7. Nawaz M, Camussi G, Valadi H, Nazarenko I, Ekstrom K, Wang X, Principe S, Shah N, Ashraf NM, Fatima F, et al. The emerging role of extracellular vesicles as biomarkers for urogenital cancers. Nat Rev Urol. 2014;11:688–701.
8. Thompson AG, Gray E, Heman-Ackah SM, Mager I, Talbot K, Andaloussi SE, Wood MJ, Turner MR. Extracellular vesicles in neurodegenerative disease—pathogenesis to biomarkers. Nat Rev Neurol. 2016;12:346–57.
9. Moldovan L, Batte K, Wang Y, Wisler J, Piper M. Analyzing the circulating microRNAs in exosomes/extracellular vesicles from serum or plasma by qRT-PCR. Methods Mol Biol. 2013;1024:129–45.
10. Tavallaie R, McCarroll J, Le Grand M, Ariotti N, Schuhmann W, Bakker E, Tilley RD, Hibbert DB, Kavallaris M, Gooding JJ. Nucleic acid hybridization on an electrically reconfigurable network of gold-coated magnetic nanoparticles enables microRNA detection in blood. Nat Nanotechnol. 2018;13:1066–71.
11. Yokoi A, Matsuzaki J, Yamamoto Y, Yoneoka Y, Takahashi K, Shimizu H, Uehara T, Ishikawa M, Ikeda SI, Sonoda T, et al. Integrated extracellular microRNA profiling for ovarian cancer screening. Nat Commun. 2018;9:4319.
12. Jiang S, Li Q, Wang C, Pang Y, Sun Z, Xiao R. In situ exosomal microRNA determination by target-triggered SERS and Fe3O4@TiO2-based exosome accumulation. ACS Sens. 2021;6:852–62.
13. Kang T, Zhu J, Luo X, Jia W, Wu P, Cai C. Controlled self-assembly of a close-packed gold octahedra array for SERS sensing exosomal microRNAs. Anal Chem. 2021;93:2519–26.
14. Miti A, Thamm S, Muller P, Csaki A, Fritzsche W, Zuccheri G. A miRNA biosensor based on localized surface plasmon resonance enhanced by surface-bound hybridization chain reaction. Biosens Bioelectron. 2020;167: 112465.
15. Wang R, Zhao X, Chen X, Qiu X, Qing G, Zhang H, Zhang L, Hu X, He Z, Zhong D, et al. Rolling circular amplification (RCA)-assisted CRISPR/Cas9 cleavage (RACE) for highly specific detection of multiple extracellular vesicle microRNAs. Anal Chem. 2020;92:2176–85.
16. Li X, Li X, Li D, Zhao M, Wu H, Shen B, Liu P, Ding S. Electrochemical biosensor for ultrasensitive exosomal miRNA analysis by cascade primer exchange reaction and MOF@Pt@MOF nanozyme. Biosens Bioelectron. 2020;168: 112554.
17. Tang X, Wang Y, Zhou L, Zhang W, Yang S, Yu L, Zhao S, Chang K, Chen M. Strand displacement-triggered G-quadruplex/rolling circle amplification strategy for the ultra-sensitive electrochemical sensing of exosomal microRNAs. Mikrochim Acta. 2020;187:172.
18. Zhou J, Lin Q, Huang Z, Xiong H, Yang B, Chen H, Kong J. Aptamer-initiated catalytic hairpin assembly fluorescence assay for universal, sensitive exosome detection. Anal Chem. 2022;94:5723–8.
19. Zhang Y, Yang G, Zhao J, He Y, Yuan R, Chen S. Dynamic 3D DNA rolling walkers via directional movement on a lipid bilayer supported by Au@Fe3O4 nanoparticles for sensitive detection of MiRNA-16. Anal Chem. 2022. https://doi.org/10.1021/acs.analchem.2c00831.
20. Zhang XW, Liu MX, He MQ, Chen S, Yu YL, Wang JH. Integral multielement signals by DNA-programmed UCNP-AuNP nanosatellite assemblies for ultrasensitive ICP-MS detection of exosomal proteins and cancer identification. Anal Chem. 2021;93:6437–45.
21. Chai SQ, Lv WY, He JH, Li YF, Zou HY, Li CM, Huang CZ. Highly sensitive detection of miR-21 through target-activated catalytic hairpin assembly of X-shaped DNA nanostructures. Anal Chem. 2021;93:14545–51.
22. Wu C, Cansiz S, Zhang L, Teng IT, Qiu L, Li J, Liu Y, Zhou C, Hu R, Zhang T, et al. A nonenzymatic hairpin DNA cascade reaction provides high signal gain of mRNA imaging inside live cells. J Am Chem Soc. 2015;137:4900–3.
23. Lv MM, Liu JW, Yu RQ, Jiang JH. A bipedal DNA nanowalker fueled by catalytic assembly for imaging of base-excision repairing in living cells. Chem Sci. 2020;11:10361–6.
24. Yang Z, Liu B, Huang T, Xie BP, Duan WJ, Li MM, Chen JX, Chen J, Dai Z. Smart hairpins@MnO2 nanosystem enables target-triggered enzyme-free exponential amplification for ultrasensitive imaging of intracellular microRNAs in living cells. Anal Chem. 2022;94:8014–23.
25. Li J, Liu S, Sun L, Li W, Zhang SY, Yang S, Li J, Yang HH. Amplified visualization of protein-specific glycosylation in zebrafish via proximity-induced hybridization chain reaction. J Am Chem Soc. 2018;140:16589–95.
26. Jung C, Ellington AD. Diagnostic applications of nucleic acid circuits. Acc Chem Res. 2014;47:1825–35.
27. Song C, Zhang J, Jiang X, Gan H, Zhu Y, Peng Q, Fang X, Guo Y, Wang L. SPR/SERS dual-mode plasmonic biosensor via catalytic hairpin assembly-induced AuNP network. Biosens Bioelectron. 2021;190: 113376.
28. Li K, Luo S, Guan S, Situ B, Wu Y, Ou Z, Tao M, Zheng L, Cai Z. Tetrahedral framework nucleic acids linked CRISPR/Cas13a signal amplification system for rare tumor cell detection. Talanta. 2022;247: 123531.
29. Wang Y, Zhao G, Chi H, Yang S, Niu Q, Wu D, Cao W, Li T, Ma H, Wei Q. Self-luminescent lanthanide metal-organic frameworks as signal probes in electrochemiluminescence immunoassay. J Am Chem Soc. 2021;143:504–12.
30. Wu Y, Zhang Y, Zhang X, Luo S, Yan X, Qiu Y, Zheng L, Li L. Research advances for exosomal miRNAs detection in biosensing: from the massive study to the individual study. Biosens Bioelectron. 2021;177: 112962.
31. Peng S, Tan Z, Chen S, Lei C, Nie Z. Integrating CRISPR-Cas12a with a DNA circuit as a generic sensing platform for amplified detection of microRNA. Chem Sci. 2020;11:7362–8.
32. Zhang G, Han Q, Song L, Liu P, Kuang G, Fu Y. Oxidized plant leaf-derived carbon dots as novel electrochemiluminescent luminophores for ultrasensitive microRNA-21 detection. Sens Actuators B Chem. 2021. https://doi.org/10.1016/j.snb.2021.130529.
33. Zhang Y, Zhang X, Situ B, Wu Y, Luo S, Zheng L, Qiu Y. Rapid electrochemical biosensor for sensitive profiling of exosomal microRNA based on multifunctional DNA tetrahedron assisted catalytic hairpin assembly. Biosens Bioelectron. 2021;183: 113205.
34. Shi Y, Wang Z, Zhu X, Chen L, Ma Y, Wang J, Yang X, Liu Z. Exosomal miR-1246 in serum as a potential biomarker for early diagnosis of gastric cancer. Int J Clin Oncol. 2020;25:89–99.
35. Wei C, Li Y, Huang K, Li G, He M. Exosomal miR-1246 in body fluids is a potential biomarker for gastrointestinal cancer. Biomark Med. 2018;12:1185–96.

Publisher's Note